*Research Article*

# Characteristics of Braced Excavation under Asymmetrical Loads

## Changjie Xu, Yuanlei Xu, Honglei Sun, and Qizhi Chen

*Research Center of Coastal and Urban Geotechnical Engineering, College of Civil Engineering and Architecture, Zhejiang University, Hangzhou 310058, China*

Correspondence should be addressed to Honglei Sun; saitholy@gmail.com

Numerous excavation practices have shown that large discrepancies exist between field monitoring data and calculated results when the conventional symmetry-plane method (with half-width) is used to design the retaining structure under asymmetrical loads. To examine the characteristics of a retaining structure under asymmetrical loads, we use the finite element method (FEM) to simulate the excavation process under four different groups of asymmetrical loads and create an integrated model to tackle this problem. The effects of strut stiffness and wall length are also investigated. The results of numerical analysis clearly imply that the deformation and bending moment of diaphragm walls are distinct on different sides, indicating the need for different rebar arrangements when the excavation is subjected to asymmetrical loads. This study provides a practical approach to designing excavations under asymmetrical loads. We analyze and compare the monitoring and calculation data at different excavation stages and find some general trends. Several guidelines on excavation design under asymmetrical loads are drawn.

## 1. Introduction

The development of urban construction and the exploitation of underground space have intensified the complexity of excavation projects, such as deep excavation, different depth excavation, and excavation under asymmetric external loads. Most deep excavations in coastal areas are supported by a retaining strutting system, which has been extensively investigated. Li et al. [1] simplified the excavation as a plane issue using displacement iteration to analyze the internal force and deformation of the retaining structure. Chen et al. [2] and Liu and Zeng [3] used FLAC3D to simulate the excavation process and drew useful conclusions on the service ability of the retaining structure. Gharti et al. [4] developed a numerical procedure based on the spectral element method, employing the linear elastic constitutive model for excavation simulations. A drawback of these studies, whether using the conventional design methods or the FEM approaches, is that they all neglected the integrated work of the whole retaining strutting system. Moreover, the excavation design is based on beams on elastic foundation method and a conventionally simplified plane-strain excavation model with one side, assuming equal loads on both sides of the excavated pit; that is, $P_1 = P_2$, as schematically shown in Figure 1,

where $P_1$ and $P_2$ are two design loads acting on different sides of the ground surface. Widely used in practice, although this method (i.e., symmetrical semiplane method) is simple but satisfies most excavation designs. When $P_1 \neq P_2$, the axial forces in the supporting struts become different; that is, $F_1 \neq F_2$, and it is contradictory to the assumption of symmetry condition. Designing excavations by conventional methods results in two extreme consequences: (a) reduced safety factor when the pit side with smaller loads is selected or (b) conservative and wasteful results when the larger load side is selected. The latter is satisfied only from the perspective of integral stability, but this method inaccurately predicts the deflection of retaining structures.

Given the diversity of geological conditions in the soil strata, the complication of excavation surroundings, and the uncertainty of construction factors, asymmetrical loads on two sides of an excavation site have become increasingly common. Asymmetrical loads, especially those of sites in downtown areas, are easily brought about by buildings and traffic loads nearby. These loads have created challenges to the conventional symmetry-plane design method, which cannot consider the integral work of foundation pits under asymmetrical loads. Lv et al. [5] introduced the geotechnical and tunnel analysis system (GTS) program to analyze the
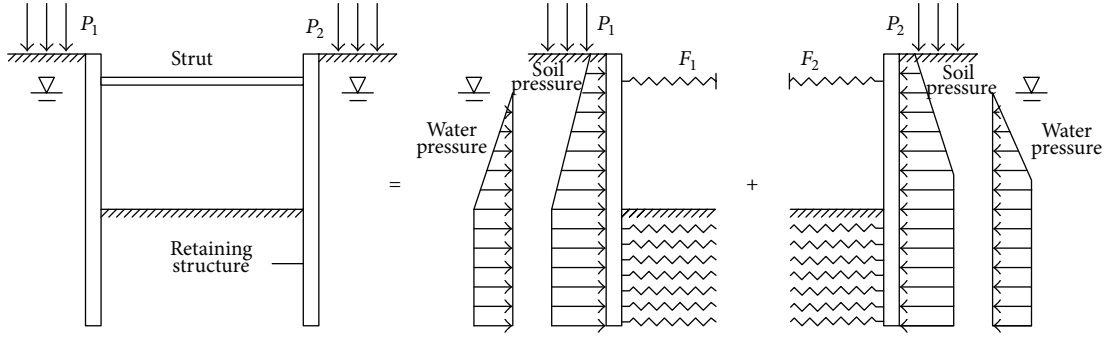
FIGURE 1: Schematic diagram for the calculation of conventional design method.

behavior of deep foundation pits under asymmetrical load, which was a part of Suzhou Metro Line 1, and drew conclusions from the simulated construction. Xu [6] and Wu [7] used the Winkler model to analyze the properties of the retaining structure of foundation pits with asymmetrical loads nearby, but oversimplified analysis and the limitation of beams on elastic foundation method prevented their findings from being widely used in engineering practice.

In the present work, a numerical investigation by PLAXIS is carried out to simulate the deformation and internal force of retaining structures under four different groups of asymmetrical loads ($P_1$ on the left and $P_2$ on the right: $P_1 = P_2 = 15$ kPa; $P_1 = 2P_2 = 30$ kPa; $P_1 = 3P_2 = 45$ kPa; $P_1 = 4P_2 = 60$ kPa). The effects of strut stiffness and diaphragm wall length are also investigated. Data comparisons between the monitoring and asymmetry integrated method and the conventional symmetry method confirm that the proposed asymmetry integrated method is a reliable and economical method for designing asymmetrical load excavations because it accounts for the connections between the diaphragm wall and strut under the asymmetrical loads. Several general conclusions are drawn regarding the design of excavations under asymmetrical loads.

## 2. Simulation of the Excavation Process under Asymmetrical Loads

*2.1. Introduction to FE Analysis.* The hardening soil (HS) [8, 9] model first proposed by Schanz et al. [10] is applied to the numerical analyses by PLAXIS. The HS model is an elastoplastic hyperbolic model formulated in the framework of friction hardening plasticity that accounts for soil dilatation [11]. This second-order model also involves compression hardening to simulate the irreversible compaction of soil under primary compression. The HS model can be used to simulate the behavior of sand, gravel, and soft soils, such as clay and silt. The application of this model to engineering is also extensive; it can be used for dam filling, bearing capacity of ground, slope stability analysis, and foundation pit excavation [12, 13]. In this model, the cap type yield surface is employed and defined as

$$f^c = \frac{q^2}{\alpha^2} - p^2 - p_p^2,  \tag{1}$$

where $\alpha$ is the factor of cap characteristic and $p_p$ is the pre-consolidation stress:

$$q = \sigma_1' + (\delta - 1)\sigma_2' + \delta\sigma_3',$$
$$\delta = \frac{3 + \sin\varphi}{3 - \sin\varphi},  \tag{2}$$
$$p' = \frac{1}{3}\left(\sigma_1' + \sigma_2' + \sigma_3'\right).$$

The basic feature of the HS model is that the soil stiffness depends on the stress. The relation of stress and strain in the HS model is expressed as

$$E_{\text{oed}} = E_{\text{oed}}^{\text{ref}}\left(\frac{\sigma}{p^{\text{ref}}}\right)^m.  \tag{3}$$

The HS model has 11 parameters: three strength parameters of Mohr-Coulomb (effective cohesion $c$, effective angle of internal fraction $\varphi_{\text{ur}}$, and angle of dilatation $\psi$), three basic stiffness parameters (reference secant stiffness of triaxial drained test $E_{50}^{\text{ref}}$, reference secant stiffness of consolidation test $E_{\text{oed}}^{\text{ref}}$, and correlation exponent $m$), and five advanced parameters (modulus of unloading and loading $E_{\text{ur}}^{\text{ref}}$, Poisson's ratio of unloading and reloading $\mu$, reference stress $p^{\text{ref}}$, failure ratio $R_f$, and the lateral pressure coefficient under normal consolidation $K_0$). All these parameters can be measured via the conventional triaxial and consolidation tests. However, in the current study, we select the model parameters by following the procedures recommended by Schanz et al. [10] and Brinkgreve [11]. $E_{50}^{\text{ref}}$ can be obtained as follows:

$$E_{50} = E_{50}^{\text{ref}}\left(\frac{c\cos\varphi - \sigma_3'\sin\varphi}{c\cos\varphi + p^{\text{ref}}\sin\varphi}\right)^m  \tag{4}$$

in which $E_{50} = E_{\text{ref}}$, the middle stiffness of every soil layer adopted in Mohr-Coulomb model; $p^{\text{ref}} = 100$ kPa; $m = 1.0$ for clay and ~0.5 for sands and silt soil [14, 15]; $\sigma_3'$ is negative for compression, and $E_{\text{oed}}^{\text{ref}} = E_{50}^{\text{ref}}$, $E_{\text{ur}}^{\text{ref}} = 3E_{50}^{\text{ref}}$. Zhong [16] conducted triaxial consolidation tests and found that, for sandy soil, $E_{\text{ur}}^{\text{ref}} = 3 \sim 5E_{50}^{\text{ref}}$, and, for cohesive soil, $E_{\text{ur}}^{\text{ref}} = 4 \sim 6E_{50}^{\text{ref}}$. The model parameters used in the simulations are described in detail in Table 1.

TABLE 1: Soil properties at the construction site.

| Soil layers | Depth (m) | $\gamma$ (kN/m$^3$) | $E_{50}^{ref}$ (Mpa) | $E_{oed}^{ref}$ (Mpa) | $E_{ur}^{ref}$ (Mpa) | Poisson's ratio | $c$ (kPa) | Angle of internal fraction (°) | Angle of dilatation (°) |
|---|---|---|---|---|---|---|---|---|---|
| Plane fill | 3 | 18.1 | 8 | 8 | 24 | 0.30 | 1 | 30.7 | 0 |
| Clay | 8 | 20 | 4 | 4 | 18 | 0.32 | 4 | 25 | 0 |
| Sandy silt | 3.2 | 21 | 10 | 10 | 35 | 0.30 | 1 | 32 | 3 |
| Silty clay with sand | 2 | 20.7 | 3.5 | 3.5 | 16.5 | 0.33 | 3 | 26 | 1 |
| Sandy silt | — | 20 | 14 | 14 | 52 | 0.30 | 1 | 34 | 4 |



- ● Node
- × Stress point

(a) Six-node soil element

- ● Node
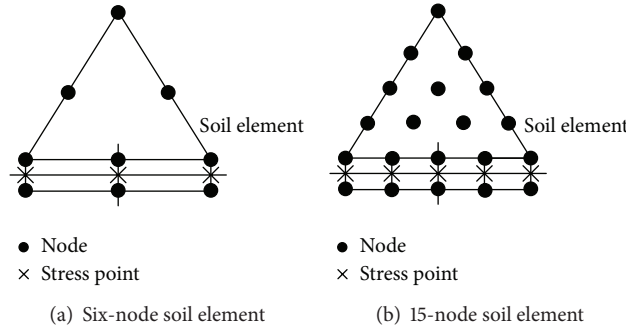- × Stress point

(b) 15-node soil element

FIGURE 2: Connection between interface and soil elements.

The calculation model adopted in this study is a two-dimension model. The 15-node element with 12 Gauss points, plate element, and anchor element are used to simulate the soil, retaining structure, and strut, respectively. According to the Mohr-Coulomb elastoplastic model, plate elements are connected to surrounding soil elements with interface elements. The interface element stiffness matrix is obtained through Newton Cotes integration. The node number of the interface element is related to that of the soil element.

As shown in Figure 2, the interface element has finite thickness, but the coordinates of each node group are equal in the finite element formula, indicating that the element thickness is zero.

*2.2. A Brief Introduction of Excavation.* Red Stone Central Park is located near the crossing of Hushu South Road and Chaowang Road. The main properties of the soil layers of the construction site are shown in Table 1. The shape of the foundation pit of the park is an approximate rectangle 95 m long and 35 m wide. The average excavation depth is 9 m. The excavation is supported by 800 mm diaphragm wall and two steel struts at 1 m and 5 m below the ground surface, respectively. The elastic modules of the diaphragm wall and steel strut are $3.0 \times 10^4$ and $2.1 \times 10^5$ MPa, respectively. The ground water level is at 2 m below ground surface, and dewatering is not considered. Typical cross section of the retaining strutting system is shown in Figure 3.

*2.3. Description of FE Model Simplification Adopted.* The calculation model, instead of the symmetry semi plane, is integrated to consider the interaction of both walls caused by the struts and passive soil area. The model is 80 m wide and 35 m deep. The horizontal displacement is restrained at

the left and right boundaries, and the vertical and horizontal displacements are fixed at the bottom (Figure 4). These boundary conditions are consistent with the initial self-weighting deformation condition of the soil.

*2.4. Simulation of Excavation Stages.* The numerical simulation is conducted according to the following steps.

*Step 1.* A model of the whole site, together with the strut structure, is established.

*Step 2.* Primary geostress is balanced to establish the initial state of stress ($K_0$ stress conditions) and eliminate the stiffness of the strut structure. Thus, the strut structure element loses its activity and becomes uninvolved with the settlement caused by soil weight.

*Step 3.* Displacements of the initial stress field are set to zero.

*Step 4.* Strut structure elements are activated, and loads near the pit are applied.

*Step 5.* Stage-by-stage excavation is conducted, and the relevant strut is activated. Soil excavation is simulated by causing soil elements to lose their activity.

Excavation process is simulated in three the stages as follows ("-" denotes the level below the ground surface).

*Stage 1.* Excavation up to −2 m is performed.

*Stage 2.* One steel strut is constructed at −1 m, and excavation is conducted up to −6 m. The first strut reaches its design strength and starts to function.

*Stage 3.* The other steel strut is constructed at −5 m, and excavation continues up to −9 m, the bottom of the foundation pit.
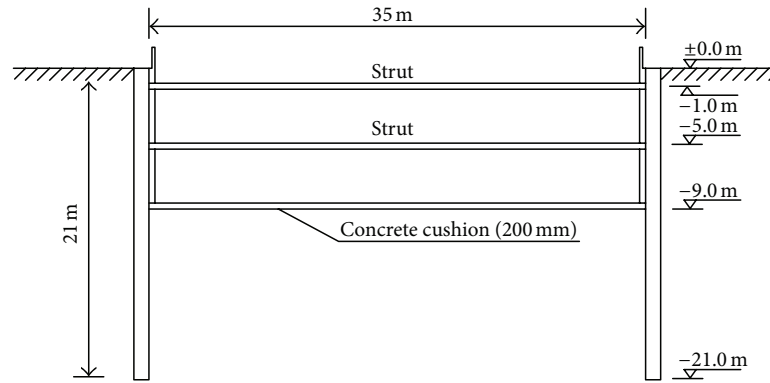
FIGURE 3: Cross section of retaining strutting system.


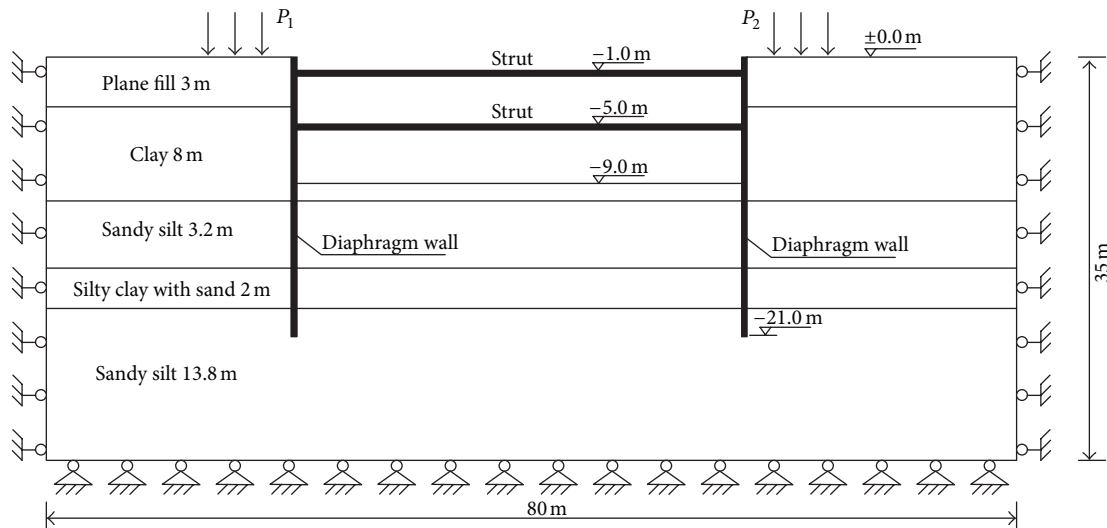
FIGURE 4: Model simplifications.

*2.5. Numerical Results under Four Groups of Loads*

*2.5.1. Horizontal Displacement.* In Stage 1, the calculated data on the left and right walls under four groups of asymmetrical loads are shown in Figure 5.

The following observations are summarized as follows.

(a) The maximum horizontal displacements on both sides occur on top of the walls.

(b) The horizontal displacement of the left wall grows with $P_1$. When $P_1$ increases from 15 kPa to 60 kPa, the maximum horizontal displacement of the left wall $S_1$ is growing from 4.05 mm to 15.03 mm.

(c) On the right side, $P_2$ is kept constant at 15 kPa. The deformation of the right wall is far less severe than that of the left wall. With increased $P_1$, the passive earth pressure transferred to the right wall rises, effectively restraining the deformation of the right wall toward the excavation. When $P_1$ increases from 15 kPa to 60 kPa, the maximum horizontal displacement of the right wall $S_2$ decreases from 4.05 mm to 2.36 mm.

The displacements for Stage 2 are shown in Figure 6.

The following observations are summarized as follows.

(a) As the first strut starts to function, the horizontal displacement is restrained. The initial cantilever movements of the wall represent a very large component of the lateral displacement of the wall for shallow cuts.

(b) With increase in $P_1$, the ability of the brace system to constrain deformation is weakened. When $P_1$ = 15 kPa, $S_1$ is 7.42 mm and appears 2 m above the excavation surface. When $P_1$ = 60 kPa, $S_1$ is 20.50 mm and occurs on top of the wall.

(c) $S_2$ is smaller than $S_1$ due to the restraint function of the strut. The larger the $P_1$, the smaller the deformation of the right wall toward the excavation. The general increased deformation of the right wall in Stage 2 is smaller than that in Stage 1. Moreover, when $P_1$ = 60 kPa, a 2.26 mm reversed horizontal displacement (outwards the excavation) appears on top of the right wall.

By Stage 3, excavation is completed. The horizontal displacements are given in Figure 7.

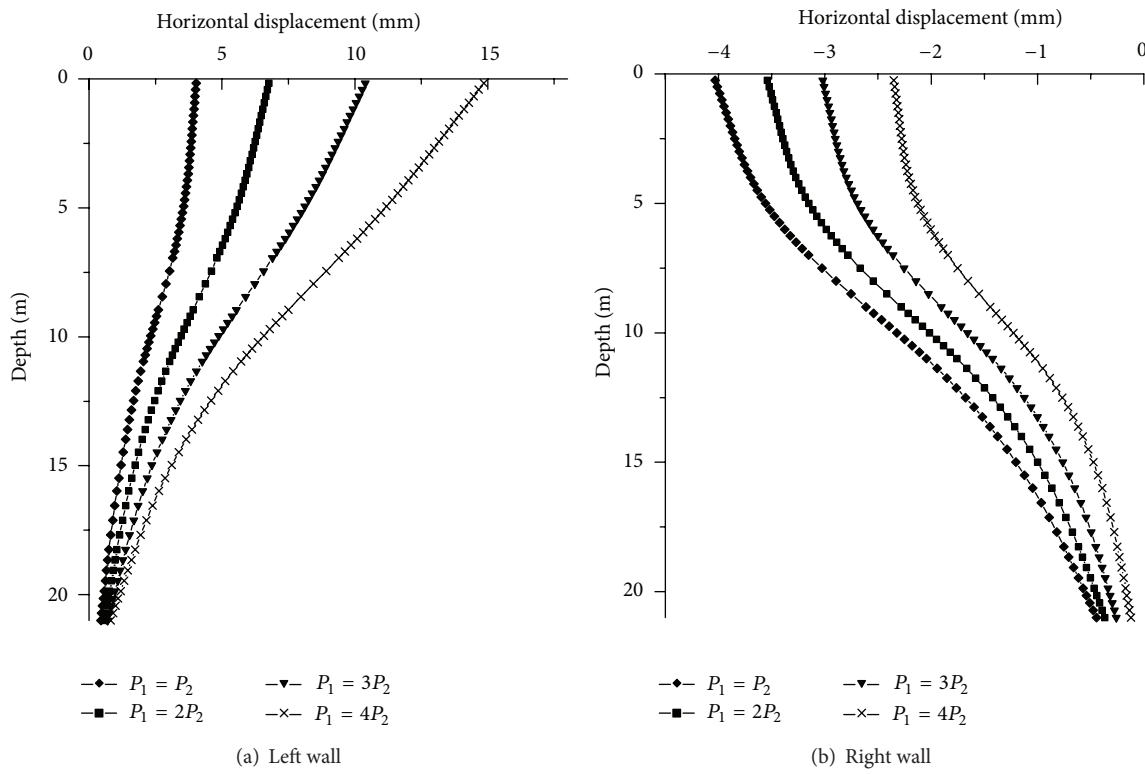The following observations are summarized as follows.

(a) Left wall

(b) Right wall

Figure 5: Horizontal displacement of diaphragm wall under different load groups (stage 1).



(a) Left wall

(b) Right wall

Figure 6: Horizontal displacement of diaphragm wall under different load groups (stage 2).
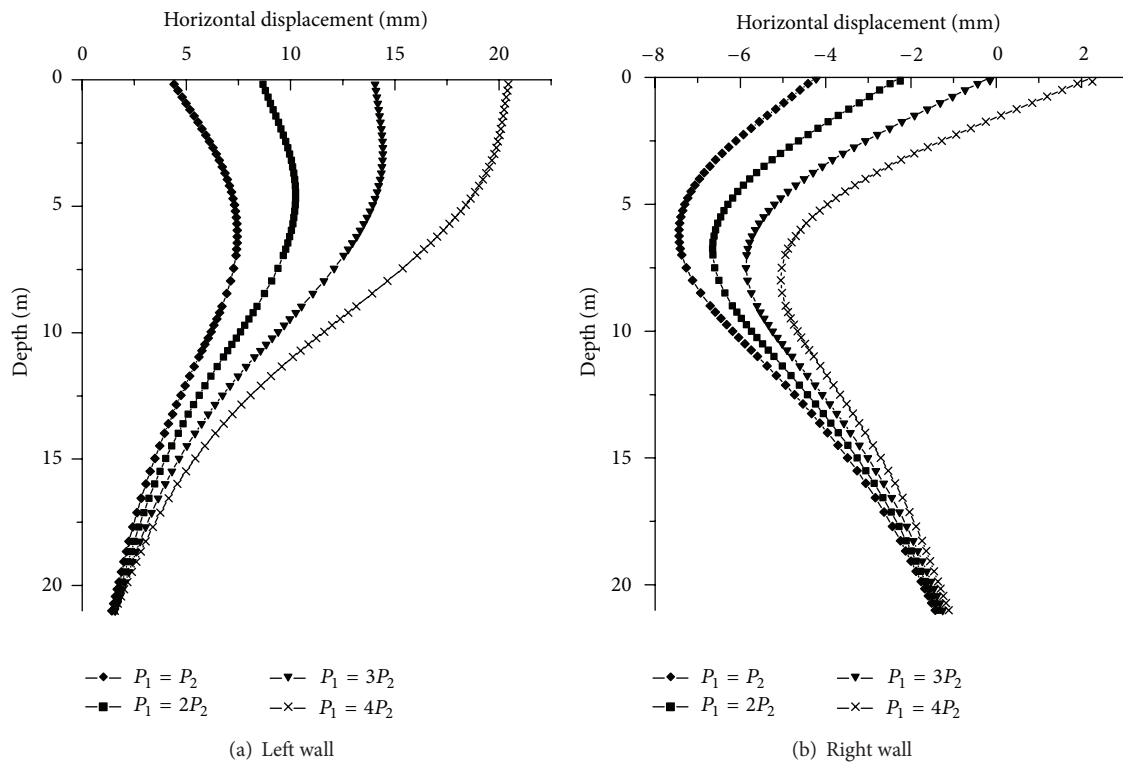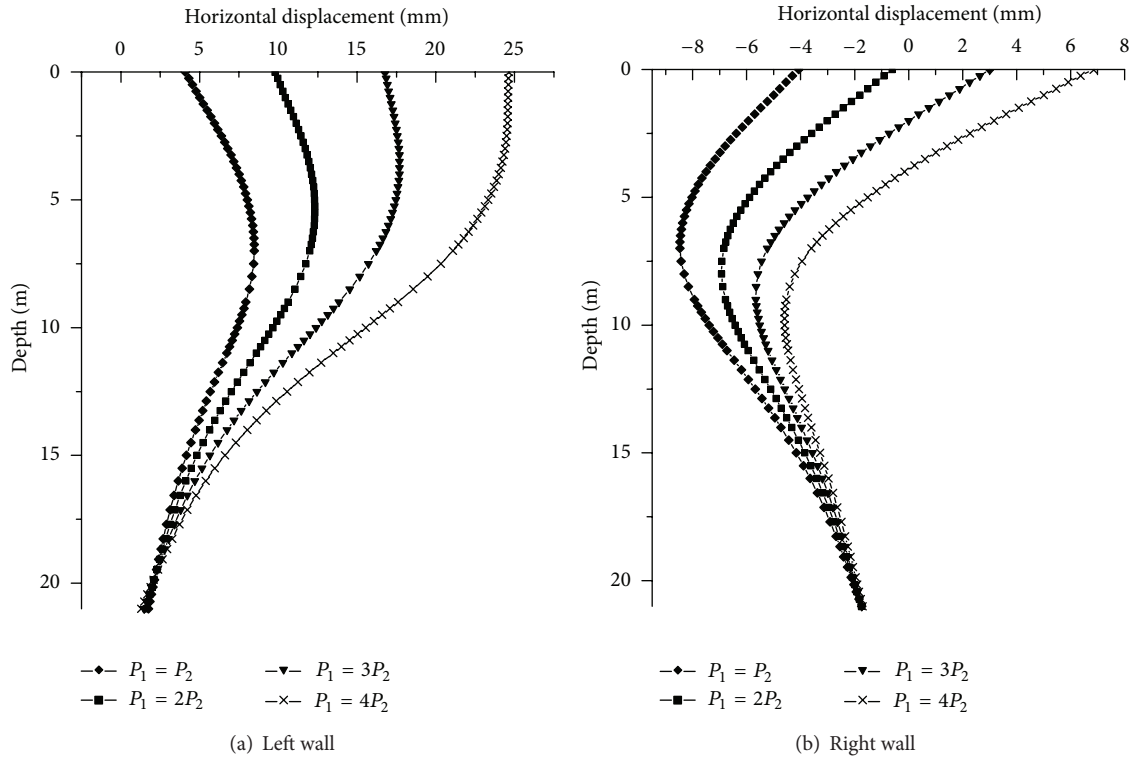
(a) Left wall

(b) Right wall

FIGURE 7: Horizontal displacement of diaphragm wall under different load groups (stage 3).

(a) The maximum horizontal displacements of both walls move to the bottom of the pit, except the group of $P_1$ = 60 kPa and $P_2$ = 15 kPa. The maximum values of $S_1$ and $S_2$ of this group are achieved on top of the wall. In general, the deformation caused by Stage 3 is smaller than those in previous stages, illustrating the effective restriction of the two-strut retaining system.

(b) In the left wall, as $P_1$ increases from 15 kPa to 60 kPa, $S_1$ increases from 8.47 mm to 24.63 mm, whereas $P_2$ remains constant. Given the increased excavation depth, reverse horizontal displacement appears earlier (when $P_1$ = 45 kPa) than Stage 1 (when $P_1$ = 60 kPa). At $P_1$ = 60 kPa, reversed displacement reaches 6.83 mm.

*2.5.2. Bending Moment.* The maximum bending moments of the different stages are shown in Figure 8.

Some observations can be summarized as follows.

(a) In Stage 1, with increased $P_1$ on the left side, the magnitude of the bending moment increases from 57.65 kN·m/m to 121.00 kN·m/m. The bending moment on the right side varies slightly regardless of the variation in $P_1$. With the increasing gap between $P_1$ and $P_2$, the difference of the bending moment of the two sides becomes more obvious.

(b) In Stage 2, as $P_1$ on the left wall rises from 15 kPa to 60 kPa, the maximum bending moment changes from 200.74 kN·m to 361.35 kN, signifying an 80% increase. The maximum bending moment of the
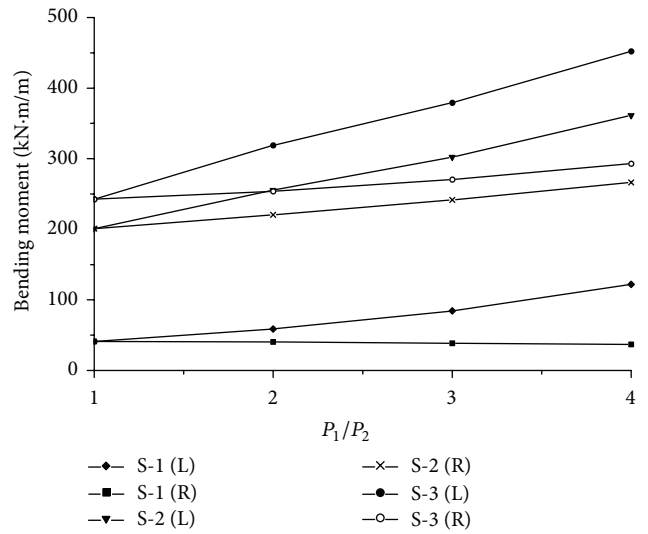


FIGURE 8: Maximum bending moment of multiple stages (S: stage; L: left; R: right).

right wall changes from 200.74 kN·m to 266.25 kN·m, indicating a 32.6% growing. Compared with that in Stage 1, the gap between the left and right walls narrows as excavation depth increases.

(c) In Stage 3, with increased $P_1$, the magnitudes of the left and right walls increasingly vary. During excavation, the discrepancy between the bending moment of the left wall and that of the right first increases and
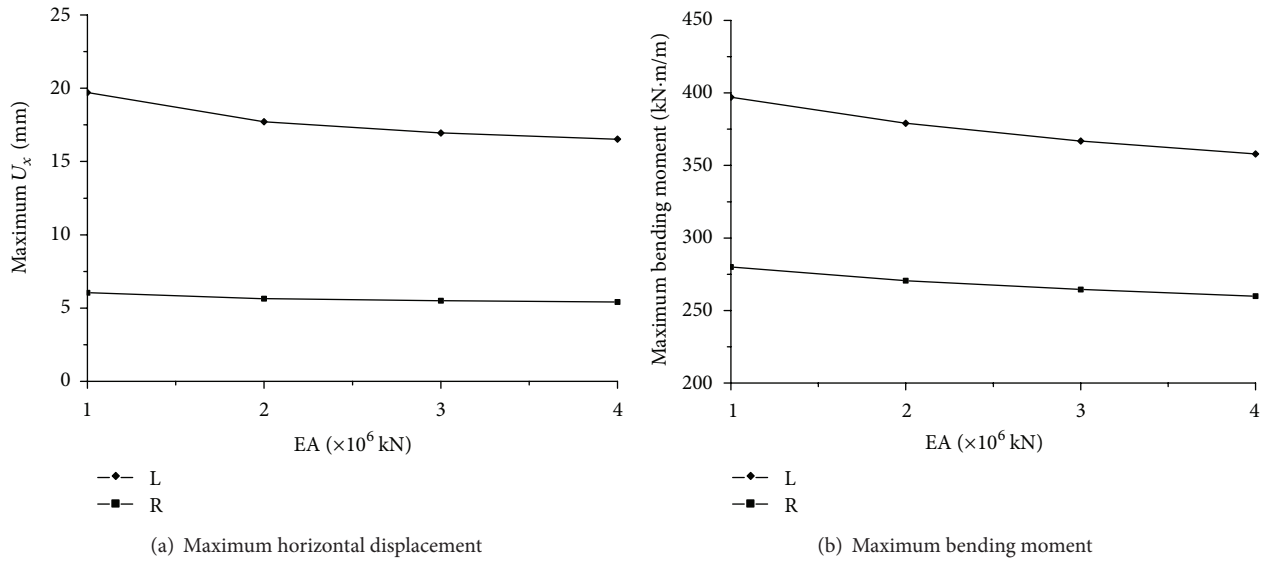
(a) Maximum horizontal displacement

(b) Maximum bending moment

FIGURE 9: Relationship between diaphragm wall characteristics and strut stiffness (L: left; R: right).



(a) Maximum horizontal displacement
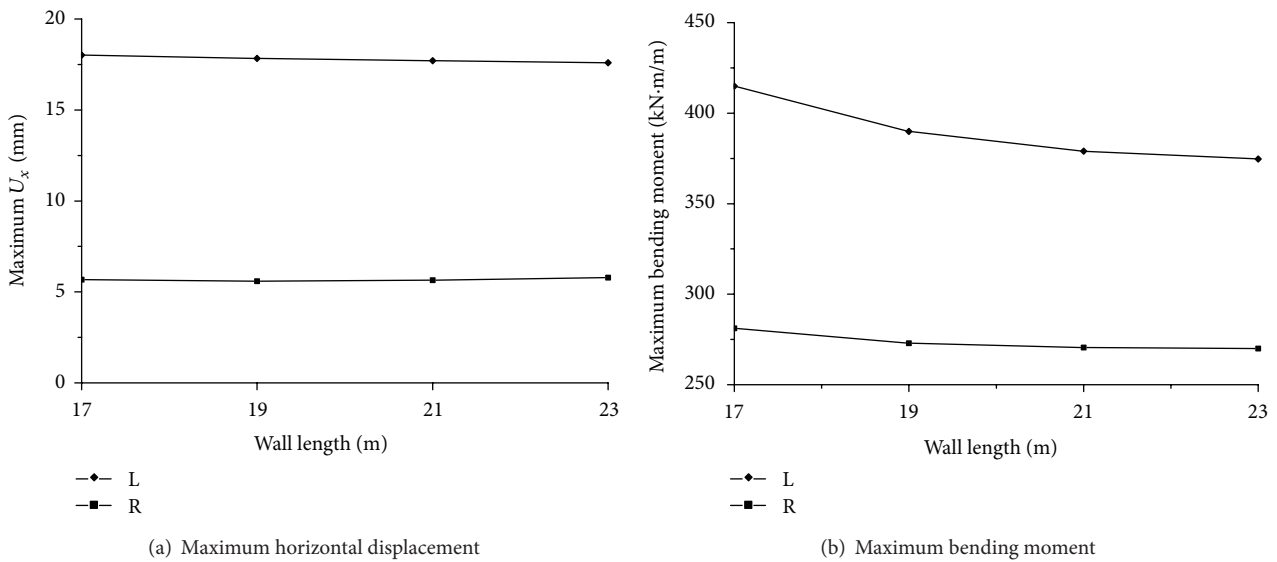
(b) Maximum bending moment

FIGURE 10: Relationship between diaphragm wall characteristics and wall length (L: left; R: right).

then decreases. The asymmetrical characteristic of the retaining structure is not proportional to excavation depth.

### 2.6. Effect of Strut Stiffness.

Strut stiffness is directly related to wall deflection and bending moment distribution. The characteristics of wall deflection and maximum bending moment are investigated under the asymmetrical loads $P_1 = 3P_2 = 45$ kPa, with strut stiffness (EA) varying from $1 \times 10^6$ kN to $4 \times 10^6$ kN. The maximum horizontal displacement and bending moment of the diaphragm walls in Stage 3 are plotted in Figure 9.

With increased strut stiffness, the discrepancy between the left and right walls narrows. When EA increases from $1 \times 10^6$ kN to $2 \times 10^6$ kN, the maximum horizontal displacements

of the left and right walls are reduced by 10.23% and 10.59%, respectively. The increasing EA does not have a significant effect. Based on the inner force, appropriately increasing strut stiffness reduces diaphragm wall rebar and saves cost.

### 2.7. Effect of Diaphragm Wall Length.

Figure 10 compares the maximum horizontal displacement and bending moment of the Stage 3 walls, which has diaphragm wall lengths of 17, 19, 21, and 23 m and embedded lengths of 8, 10, 12, and 14 m, respectively. The asymmetrical loads are $P_1 = 3P_2 = 45$ kPa. The strut conditions remain the same.

The extension of wall length significantly affects the magnitude of the bending moment, and the maximum bending moment of both walls decreases. The left diaphragm wall
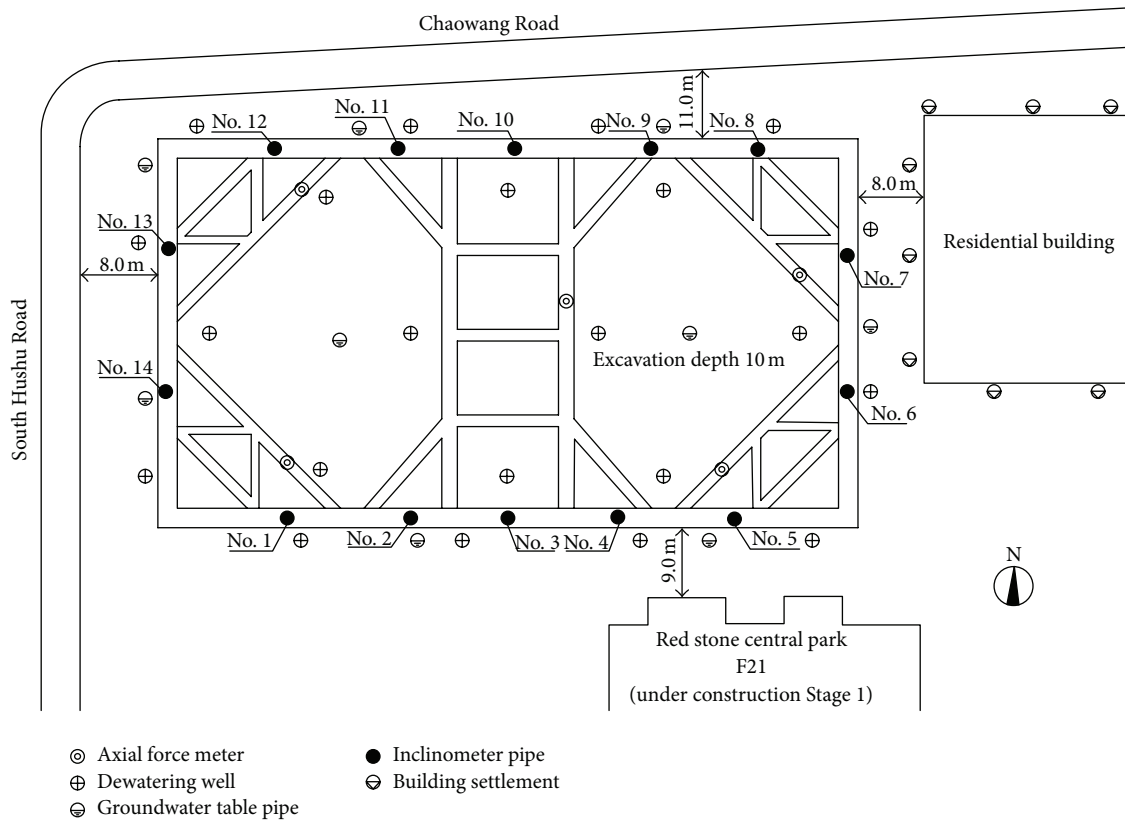
Figure 11: Layout of field monitoring.

is reduced by 3.92% and the right wall by 1.12%. However, maximum horizontal displacement is only slightly affected.

## 3. Comparison of Integrated Method and Observation Data

General information is described in *A brief introduction of excavation*. Strut stiffness is $2 \times 10^6$ kN, and diaphragm wall length is 21 m. Given the limitation of the construction site, the raw materials and construction machineries are stacked near the edge of the pit. As a result, the load on the left side is 45 kPa and on the right 15 kPa approximately. To highlight the advantage of the asymmetry integrated method, we present the results of the symmetry semiplane calculation below ($P_1$ = 45 kPa for left diaphragm wall, $P_2$ = 15 kPa for right).

*3.1. Comparisons of Horizontal Displacement.* To verify the applicability of the asymmetrical integrated design, we measure the horizontal displacement of the walls every 1 m along the depth at the end of each stage. One portion of the field monitoring locations is shown in Figure 11, and the measurements from inclinometer pipes of No. 3 and No. 10 are compared with numerical data.

Shown in Figure 12 is comparison of horizontal displacements.

It is seen that with an excavation depth of 2 m (Stage 1), the calculation data of the symmetry semiplane method (15

or 45 kPa) are not much different from the monitoring data. Through the asymmetry integrated method, the calculation and monitoring data are generally consistent from Stage 1 to Stage 3. The magnitude of $S_1$ is larger than the symmetry semiplane calculation results in all stages (however, the load is 15 or 45 kPa). This discrepancy illustrates that the symmetry loads on both sides facilitate the deformation control of sides with larger loads. In practice, the horizontal deformation of the right wall is well restrained.

The deformation of soil surrounding the excavation significantly affects buildings and pipes nearby. This deformation is closely related to the horizontal deformation of the diaphragm wall. Therefore, the horizontal deformation of the wall should be predicted as accurately as possible. Thus, the asymmetry integrated method is recommended.

*3.2. Comparisons of Bending Moment.* To obtain the bending moment, rebar stress gauges are deployed by being connected with the main rebar every two meters along the depth before wall construction. The positions of the gauges on the north and south walls are shown in Figure 13. Such gauges are placed on both wall interior and exterior to measure the positive and negative bending moment. Seventy-two rebar stress gauges are deployed. The stresses are recorded at the end of each stage.

Figure 14 shows the comparison graphs of stresses. In general, the calculated data match the monitoring data in Stage 1 with the semiplane method. As the excavation

(a) Left wall (Stage 1)

(b) Right wall (Stage 1)

(c) Left wall (Stage 2)

(d) Right wall (Stage 2)

(e) Left wall (Stage 3)
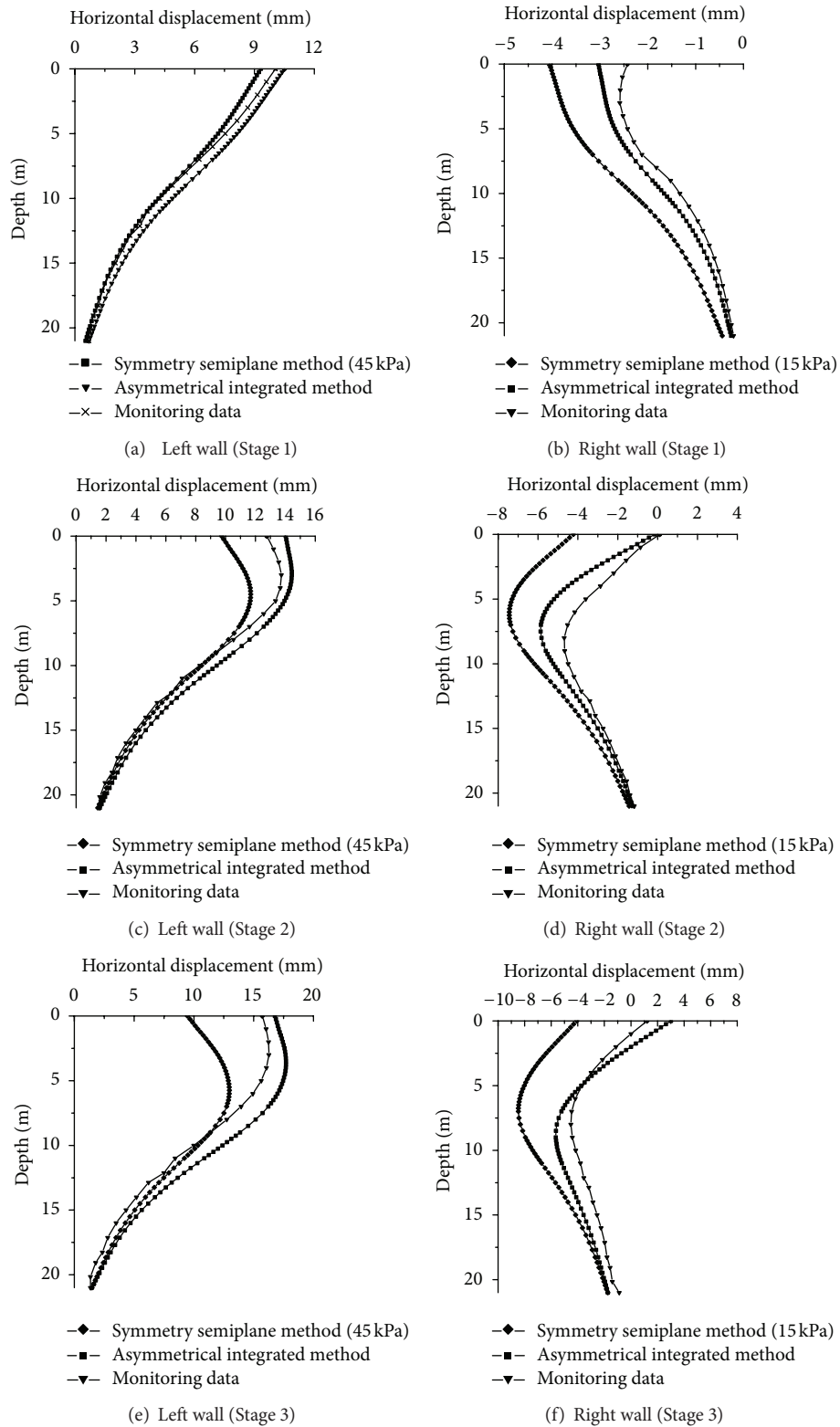
(f) Right wall (Stage 3)

FIGURE 12: Horizontal displacement of diaphragm wall with different methods and monitoring data.
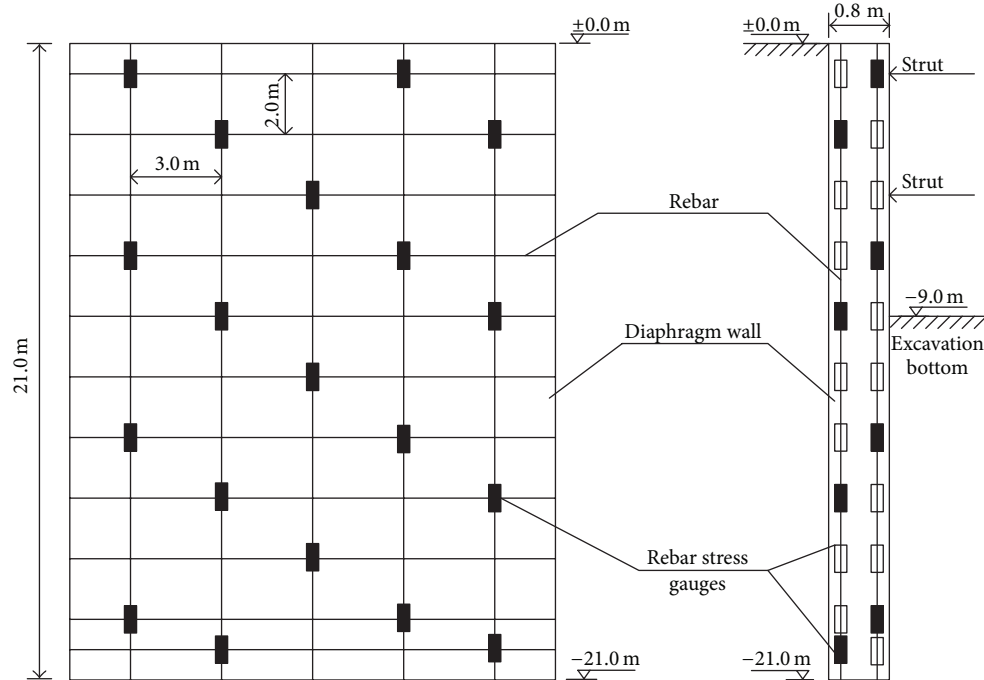
FIGURE 13: Layout of rebar stress gauges.

progresses, the semiplane method becomes too conservative for the left wall and a little risky for the right, although the discrepancy of the right wall is small. The results of the asymmetry integrated method are only marginally smaller than measured data, a difference of roughly 20%. The results are consistent probably because the locations of the stress gauges are not the exact places where the maximum bending moment occurs.

The results of rebar arrangement are shown in Table 2.

With foundation pit safety still ensured, the asymmetrical integrated design reduces the rebar requirement of the left wall by 14.8%, a remarkable economic benefit.

These results confirm the reliability of the parameters selected, and the feasibility of the proposed method in terms of horizontal displacement and bending moment.

## 4. Conclusions

The following conclusions can be drawn from this study.

(1) Increased load on one side positively affects the deformation control of the other side. When the load gap of two sides is enlarged, the side with a smaller load experiences reverse displacement on top of the wall, which is not observed with the semiplane method. The horizontal displacement of the diaphragm wall of excavations near important structures should be accurately predicted and strictly controlled because these pits have strict deformation requirements. Thus, the displacement caused by the symmetry semiplane method should not be used to forecast the horizontal displacement of the wall.

(2) When the load of one side increases, the bending moment of this side becomes significantly different, whereas changes in the other side are marginal. The positions of maximum value change as excavation depth increases. In both cases, when the larger load is more than two times the smaller load, the gap of the maximum bending moment between them is over 20%. Then, the asymmetry integrated method is necessary. In situations with no strict requirements on deformation, the semiplane method is still used for the angle of the bending moment for convenient construction.

(3) Compared with wall length, strut stiffness significantly affects the asymmetrical characteristic of the walls. Given that the quantity of the strut is far smaller than that of the diaphragm wall, increasing strut stiffness to reduce wall deflection and bending moment is more economical than increasing the length of the diaphragm wall.

(4) Based on the engineering case, symmetry-plane calculation has obvious limitations compared with the proposed asymmetry integrated method, which has better consistency with the monitoring data of both horizontal displacement and bending moment. The proposed method reflects the real mechanical properties of the retaining structure and promotes economic benefits while ensuring safety.

(5) Under asymmetric loads, the characteristic difference of walls is related to the width and length of the foundation pit as well as the load, which needs further investigation.
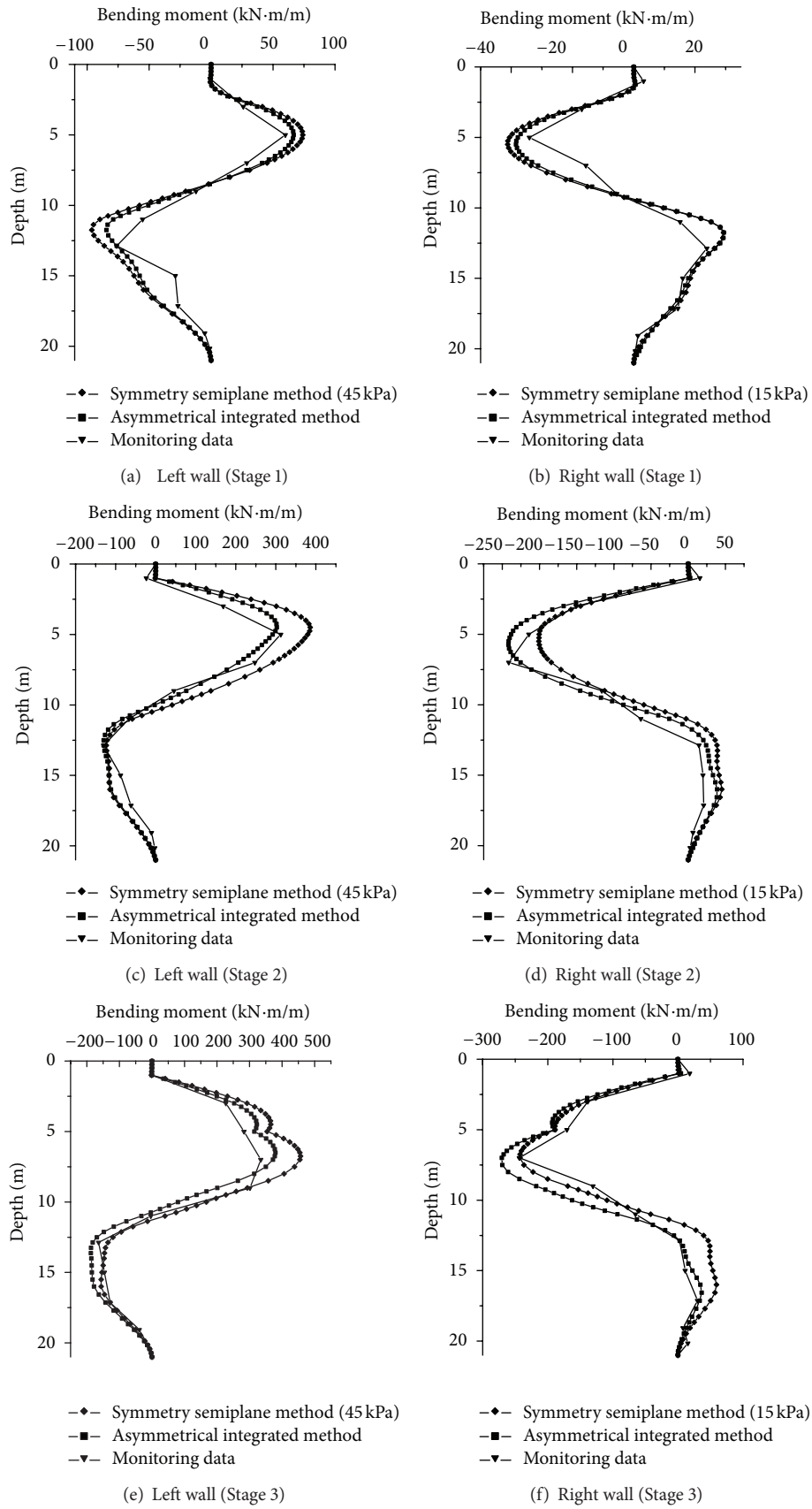
Figure 14: Bending moment of diaphragm wall under different methods and monitoring data.

TABLE 2: Comparison of symmetry-plane and asymmetrical integrated designs.

| | Left wall | | Right wall | |
| --- | --- | --- | --- | --- |
| | Maximum bending moment (kN·m/m) | Rebar | Maximum bending moment (kN·m/m) | Rebar |
| Symmetry-plane design | | | | |
| ($P_1$ = 45 kPa) | 456.7 | Φ 26@200 | — | — |
| ($P_2$ = 15 kPa) | — | — | 242.5 | — |
| Asymmetrical integrated design | | | | |
| ($P_1$ = $3P_2$ = 45 kPa) | 379.24 | Φ 24@200 | 270.61 | Φ 20@200 |

## Acknowledgments

## References

[1] P. Li, X. P. Deng, J. H. Xiang, and T. Li, "Method of displacement iteration in numerical simulation of foundation pit," *Rock and Soil Mechanics*, vol. 26, no. 11, pp. 1815–1818, 2005.

[2] M. H. Chen, Z. X. Chen, and C. S. Zhang, "Application of FLAC in analysis of foundation excavation," *Chinese Journal of Geotechnical Engineering*, vol. 28, pp. 1437–1440, 2006.

[3] J. G. Liu and Y. W. Zeng, "Application of FLAC3D to simulation of foundation excavation and support," *Rock and Soil Mechanics*, vol. 27, no. 3, pp. 505–508, 2006.

[4] H. N. Gharti, V. Oye, D. Komatitsch, and J. Tromp, "Simulation of multistage excavation based on a 3D spectral-element method," *Computers and Structures*, vol. 100-101, pp. 54–69, 2012.

[5] X. J. Lv, Q. Yang, D. L. Qian, and J. Liu, "Deformation analysis on supporting structure of deep foundation pit under the condition of asymmetric overloading," *Chinese Journal of Hefei University Technology*, vol. 35, no. 6, pp. 809–813, 2012.

[6] Z. B. Xu, *Study on deformation of foundation pit under asymmetric load [Dissertation]*, Southeast University of China, 2005.

[7] X. J. Wu, *Deformation control research on deep foundation pit of subway transfer station paralleling with the station hall [Dissertation]*, Tongji University of China, 2006.

[8] B. O. Hardin and W. L. Black, "Closure to vibration modulus of normally consolidated clays," *Journal of Soil Mechanic and Foundations Division*, vol. 95, no. 6, pp. 1531–1537, 1969.

[9] B. O. Hardin and V. P. Drnevich, "Shear modulus and damping in soils: design equations and curves," *Journal of Soil Mechanic and Foundations Division*, vol. 98, no. 7, pp. 667–692, 1972.

[10] T. Schanz, P. A. Vermeer, and P. G. Bonnier, "The hardening soil model: formulation and verification," in *Beyond 2000 in Computational Geotechnics*, pp. 281–296, Balkema, Amsterdam, The Netherlands, 1999.

[11] R. B. J. Brinkgreve, "Selection of soil models and parameters for geotechnical engineering application," in *Soil Constitutive Models, Proceedings of the Sessions of the Geo-Frontiers Congress*, pp. 69–98, ASCE, Austin, Tex, USA, 2005.

[12] Z. H. Xu and W. D. Wang, "Selection of soil constitutive models for numerical analysis of deep excavations in close proximity to sensitive properties," *Rock and Soil Mechanics*, vol. 31, no. 1, pp. 258–264, 2010.

[13] A. Tolooiyan and K. Gavin, "Modelling the cone penetration test in sand using cavity expansion and arbitrary lagrangian eulerian finite element methods," *Computers and Geotechnics*, vol. 38, no. 4, pp. 482–490, 2011.

[14] J. Janbu, "Soil compressibility as determined by oedometer and triaxial tests," *ECSMFE Wiesbaden*, vol. 1, pp. 19–25, 1963.

[15] X. L. Liu, R. Ma, G. Q. Guo, T. Tao, and H. Zhou, "Applicability of PLAXIS2D used for numerical simulation in foundation pit excavation," *Chinese Journal of Ocean University*, vol. 42, no. 4, pp. 019–025, 2012.

[16] L. Zhong, *The characteristic of retaining structure of multi-stage excavation [Dissertation]*, Fuzhou University of China, 2007.

Advances in
Operations Research

Advances in
Decision Sciences

Journal of
Applied Mathematics

Algebra

Journal of
Probability and Statistics

The Scientific
World Journal

International Journal of
Differential Equations

International Journal of
Combinatorics

Advances in
Mathematical Physics

**Hindawi**

Submit your manuscripts at
http://www.hindawi.com

Journal of
Complex Analysis

Journal of
Mathematics

Mathematical Problems
in Engineering

Abstract and
Applied Analysis

Discrete Dynamics in
Nature and Society

International
Journal of
Mathematics and
Mathematical
Sciences

Journal of
Discrete Mathematics

Journal of
Function Spaces

International Journal of
Stochastic Analysis

Journal of
Optimization